

Increasing the Energy Efficiency of Aluminum-Reduction Cells Using Modified Cathodes

PENG JIANPING,^{1,2} SONG YANG,¹ DI YUEZHONG,¹ WANG YAOWU,¹
and FENG NAIXIANG¹

1.—School of Metallurgy, Northeastern University, Shenyang 110819, People's Republic of China.
2.—e-mail: pengjp@smm.neu.edu.cn

A cathode with an inclined surface (5°) and increased bar collector height (230 mm high) was incorporated into two 300-kA industrial aluminum-reduction cells. The voltage of the cells with the modified cathode was reduced by approximately 200 mV when compared with that of a conventional cell with a flat cathode. Through the use of simulations, the reduction in the cell voltage was attributed to the cathode modification (40 mV) and a reduced electrolyte level of 0.5 cm (160 mV). As a result of reduced anode cathode distance (ACD), the ledge toe was extended to the anode shadow by 12 cm. This caused a large inverted horizontal current and a velocity increase. The ledge profile returned to the desired position when the cells were insulated more effectively, and the metal velocity and metal crest in the modified cells were reduced accordingly.

INTRODUCTION

Most primary aluminum is produced by the electrolysis of alumina through the Hall–Héroult process. This has been the dominant method for the production of aluminum for more than 120 years. An enormous amount of electrical energy is consumed during the electrolysis process. Thus, minimizing energy consumption is highly desirable. Unfortunately, the best aluminum smelters operate with an energy efficiency (ratio of theoretical energy required to actual energy provide) of approximately 50%,¹ with half of the electrical energy being wasted by Ohmic heating. The cells used in this process contain numerous conductive components, but it is the highly electrically resistive electrolyte that accounts for the largest part of the Joule heating of the cell ($\sim 5\%$).² Therefore, to reduce energy costs, the anode cathode distance (ACD) is kept as small as possible. Nevertheless, the presence of a strong electric current causes the vertical component of the magnetic field, generated by the external busbars, to interact with the horizontal current in the metal. This interaction promotes metal flow and oscillation. Therefore, significant efforts have focused on ensuring that the current and the vertical component of the magnetic field are more uniform to reduce both the metal wave and the ACD.^{3–7} Promising improvements have been reported by modifying the structure of the cells and the materials used within them.

These improvements in cell efficiency have involved indirect methods. In 2008, a modified cathode with protrusions was tested in the Chongqing Tiantai smelter in an effort to increase the flow resistance directly and demonstrated effective in reducing energy consumption.⁸ After that, different types of cathode protrusions were tested in subsequent years. The results of these modifications in industrial cells proved to be favorable, which was an important step toward reducing energy consumption. In 2015, a modified cathode with an inclined surface and increased collector bar height was designed and incorporated into two cells for testing. This modified cathode successfully lowered energy consumption without causing magnetohydrodynamic (MHD) instability.

In this article, electrothermal models are established in ANSYS to predict the thermal behavior of cells with conventional cathodes and modified cathodes. The effect of the cathode shape on the velocity is also calculated.

MODELS

The test cells consisted of 20 anode rods and 20 sets of double anodes and were operated at a line current of 300 kA. Three-dimensional (3-D) models of a slice of the cell were developed using ANSYS for estimating the electrothermal performance. The structure of the cells containing the modified

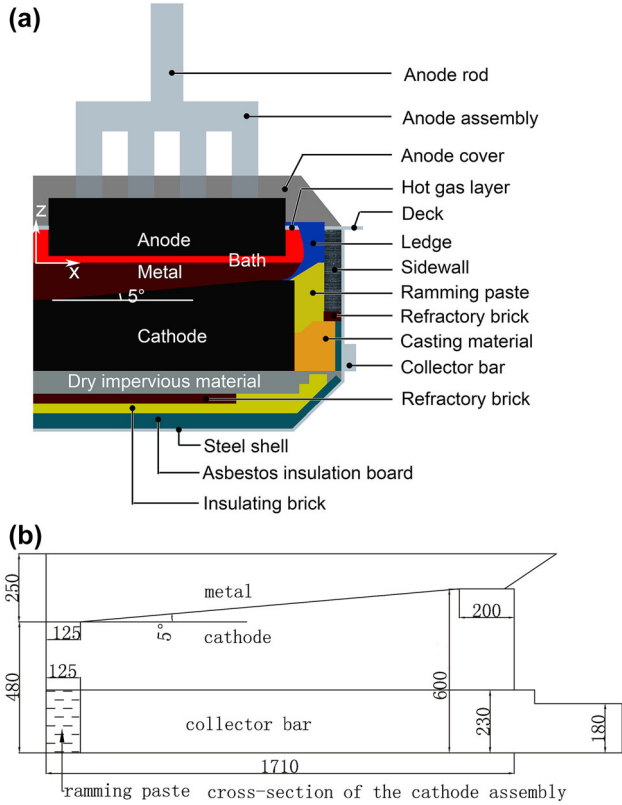


Fig. 1. (a) Structure and lining materials of an aluminum reduction cell. (b) Cathode dimensions (unit: mm).

cathodes is depicted in Fig. 1. The model of the entire cell that was used for the velocity calculation has been reported previously in the literature.⁹

The cathode modifications included an inclined cathode surface (5° inclination) and a collector bar with increased height. The height was increased from 180 mm to 230 mm over most of the collector bar length, whereas the end portion was maintained at 180 mm to match the existing cathode busbar design and to reduce heat loss.

Governing Equations

The electrothermal behavior of the cells was estimated by initially calculating the distribution of the electric potential in the conductive region. This was done by solving the Laplace equation:

$$\nabla \cdot (\sigma \nabla V) = 0 \quad (1)$$

Therefore, the current density (\mathbf{J}) was obtained using the following equation:

$$\mathbf{J} = -\sigma \nabla V \quad (2)$$

where σ is the electrical conductivity, V is the electric potential, and \mathbf{J} is the current density.

The heat transfer in each control volume is subject to the energy conservative equation (Eq. 3), which can be used to acquire the temperature distribution:

$$\rho_0 C_p \frac{\partial T}{\partial t} = \frac{\partial}{\partial x} \left[k(T) \frac{\partial T}{\partial x} \right] + \frac{\partial}{\partial y} \left[k(T) \frac{\partial T}{\partial y} \right] + \frac{\partial}{\partial z} \left[k(T) \frac{\partial T}{\partial z} \right] + \Phi \quad (3)$$

Equation 3 was used for the transient thermal analysis. At steady state, Eq. 3 simplifies to the following equation:

$$\frac{\partial}{\partial x} \left[k(T) \frac{\partial T}{\partial x} \right] + \frac{\partial}{\partial y} \left[k(T) \frac{\partial T}{\partial y} \right] + \frac{\partial}{\partial z} \left[k(T) \frac{\partial T}{\partial z} \right] + \Phi = 0 \quad (4)$$

The Ohmic heating as a volumetric source term for the thermal energy equation is given by the following equation:

$$\Phi = \sigma \nabla^2 V \quad (5)$$

The ledge profile was determined by assuming the initial ledge profile to calculate the temperature distribution and obtain the temperature nodes at the assumed ledge. These temperature nodes were then checked to see whether they fell within the temperature range of primary crystallization. The coordinates of the points on the ledge profile were then adjusted according to Eq. 6 to recalculate the temperature.¹⁰ This process was repeated until all temperature nodes satisfied the primary crystallization temperature:

$$X_{i+1} = X_i + L_{\text{step}} \times \frac{T - T_s}{T_e - T_s} \quad (6)$$

where X_i and X_{i+1} are the point coordinates at the ledge profile before and after adjustment respectively; L_{step} is the step size of a point move; T is the calculated node temperature; T_e is the electrolyte temperature; and T_s is the primary temperature of crystallization.

In a conventional cell, the ACD is approximately 5 cm. In the case of the inclined cathode, the metal height varies along the cathode length; thus, the largest metal height located at the center was kept the same 25 cm as the metal height in the conventional cell. The electrical resistivity of the electrolyte depends on its composition. In the present work, the electrical resistivity of the electrolyte was taken as 0.005 Ω m. The cathode material was 100% anthracite with an electrical resistivity of 45 $\mu\Omega$ m (20°C). The cell components properties are given in Table I.

RESULTS AND DISCUSSION

With a constant current, the voltage drop in the modified test cell was reduced by approximately 200 mV when compared with that of a conventional cell. Aside from the modified cathode, all other cell components were unchanged. Therefore, the decrease in the cell voltage drop in the modified cell may have been caused by the shape of the

Table I. Cell component properties¹¹⁻¹⁴

Component	Thermal conductivity (W/m K)	Specific thermal capacity (J/kg K)	Bulk density (kg/m ³)
Anode rod, yoke	45–0.02t	120	8000
Anode cover	$0.166 + 0.293 \times 10^{-3}(t - 27)$	1850	2400
Hot gas layer	$0.0297 + 5.25 \times 10^{-5}t$	1179	0.28
Semi-graphitic side block	$22.13 + 6.19 \times 10^{-3}t - 5.29 \times 10^{-6}t^2$	1500	1630
Anthracite side block	$5.36 + 5.81 \times 10^{-3}t - 3.43 \times 10^{-6}t^2$	1383	1580
Ramming paste	$2.98 + 2.05 \times 10^{-3}(t - 27)$	1289	1440
Refractory brick	$0.047 + 0.234 \times 10^{-3}(t + 73)$	1443	2100
Casting material	$0.3 + 1.67 \times 10^{-4}t$	950	2200
Steel collector bar	$56.6 + 0.0545 \times (t + 73)$	120	7840
Anode	$4.17 + 1.51 \times 10^{-3}t$	1354	1580
Cathode	$2.3 + 5.78 \times 10^{-3}(t - 27)$	1400	1560
Bath	1000	1760	2173
Ledge (frozen bath)	$0.825 + 0.55 \times 10^{-3}(t - 27)$	1850	2850
Molten metal	500	1088	2375
Dry impervious material	$0.31 + 6.06 \times 10^{-4}t$	900	2100
Steel shell, deck plate	45–0.02t	120	7840
Calcium silicate board	$0.047 + 0.234 \times 10^{-3}(t + 73)$	1000	220
Asbestos insulation board	$0.03 + 0.138 \times 10^{-3}t$	840	120
Insulating brick	$0.184 + 0.068 \times 10^{-3}(t + 173)$	750	425

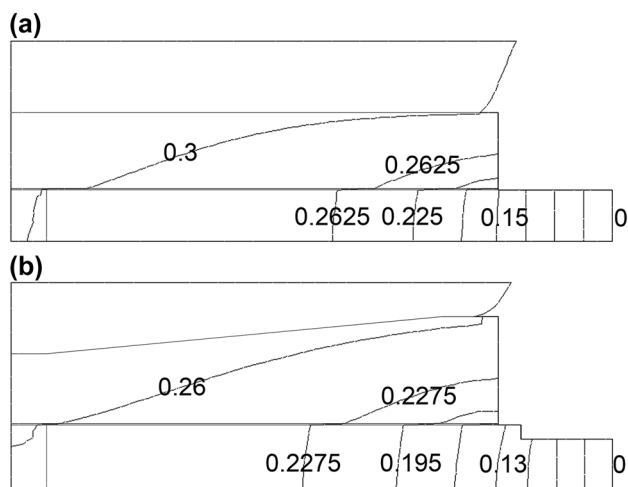


Fig. 2. Electrical potential in the cathode assembly (unit: V). (a) Flat cathode (collector bar size 65 mm × 180 mm). (b) Inclined cathode (collector bar size 70 mm × 230 mm).

modified cathode or by the reduced electrolyte level below the anodes. As the modified cathode surface could redistribute the current, which would probably affect the cathode voltage drop, the bath level was maintained to evaluate the variation in cathode voltage drop prior to determining any effect that the bath level may have had.

The voltage drop of the cathode in cells with modified cathode and conventional cathodes are compared in Fig. 2. The modified cathode caused a 40-mV reduction in the cathode voltage drop. It is

likely that the reduction in the cell voltage drop was caused by the reduced ACD. Through the use of numerical calculations, the 160-mV reduction in the voltage drop was found to correspond to an electrolyte depth of 0.5 cm. Therefore, the ACD in the modified cell was anticipated to reduce to 4.5 cm.

Temperature Distribution

A comparison of the isotherms from cross sections through the collector bar is shown in Fig. 3. The modified cell that used the same lining materials as in the conventional cell (Fig. 3b) had a lower electrolyte level, which generated less Joule heating. This caused the ledge toe to extend under the anode shadow. The isotherms shifted toward the cell interior where Joule heating was occurring. To minimize heat loss, the sidewall and bottom materials were replaced with materials with lower thermal conductivity (sidewall: semi-graphitic carbon block → amorphous carbon block [100% anthracite]; bottom: calcium silicate board → asbestos insulation board). The results predicted that the location of the bath–ledge interface was kept at a desired position after the change of insulating materials.

Consequently, to ensure sufficient heat generation for normal operation, the ACD could not be lowered too much. Aside from MHD stability, Joule heating is a major constraint for reducing the ACD. The extent of its reduction is associated with the thermal balance of the cell and magnetohydrodynamic (MHD) stability, which relies on plant trial data because of the complicated interactions that occur during the electrolysis process.

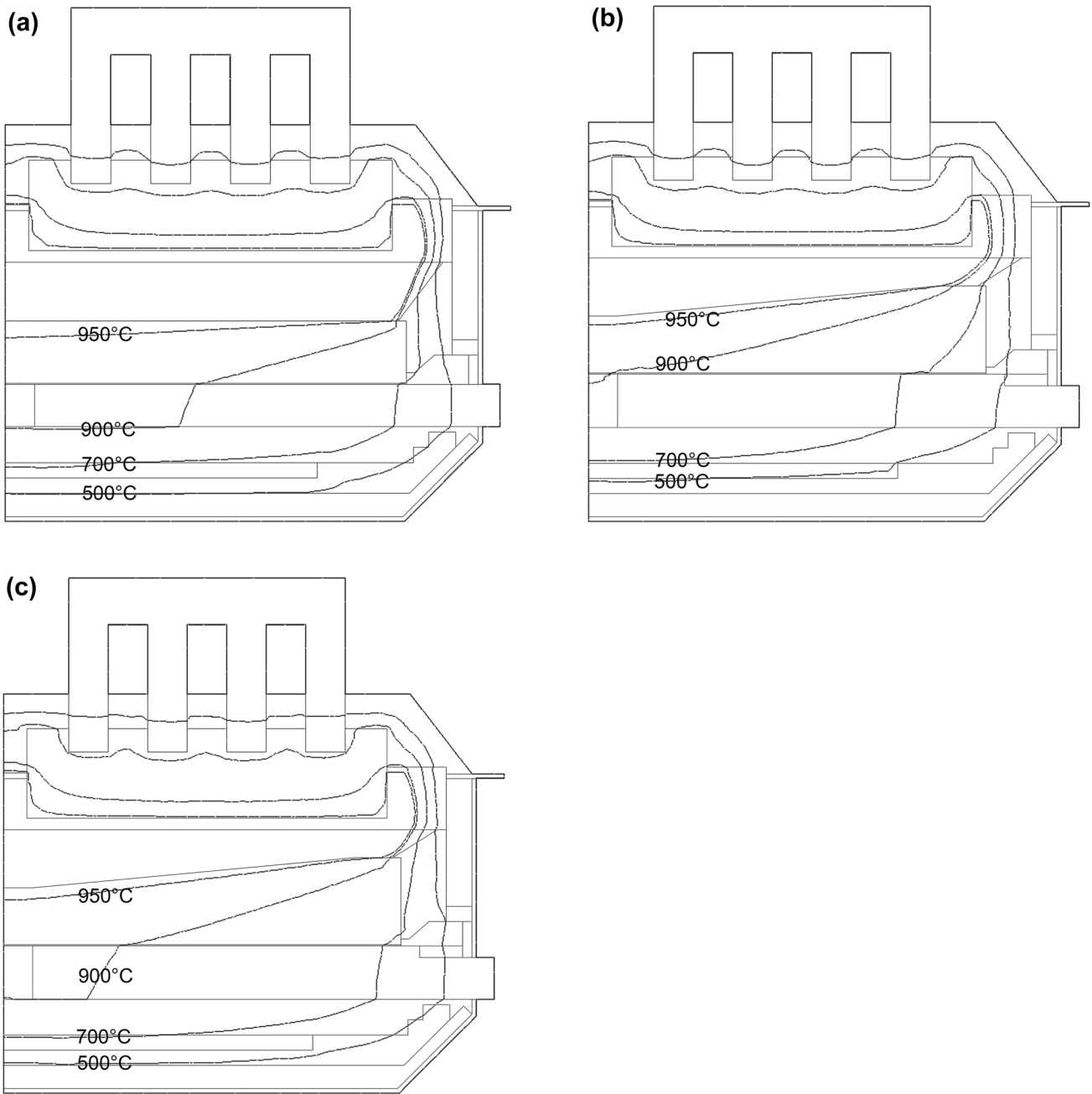


Fig. 3. Isotherms predicted for the cell. (a) Flat cathode (ACD = 5 cm). (b) Inclined cathode (ACD = 4.5 cm). (c) Inclined cathode (ACD = 4.5 cm, enhanced thermal insulation of sidewall).

Horizontal Current

The current vector in the cathode assembly is shown in Fig. 4. The current traveled via different pathways depending on the ledge profile. The extension of the ledge toe (Fig. 4b) introduced a large inverted horizontal current in the metal with a magnitude of approximately 7000 A/m^2 . This type of ledge toe extension should always be prevented during operation.

Metal Velocity

The whole cell velocity was calculated to determine the effect of the cathode shape and ledge profile.

The metal velocity of a cross section located in the middle of the entire cell is shown in Fig. 5. The inclined surface significantly reduced the metal velocity close to the cathode surface. In close

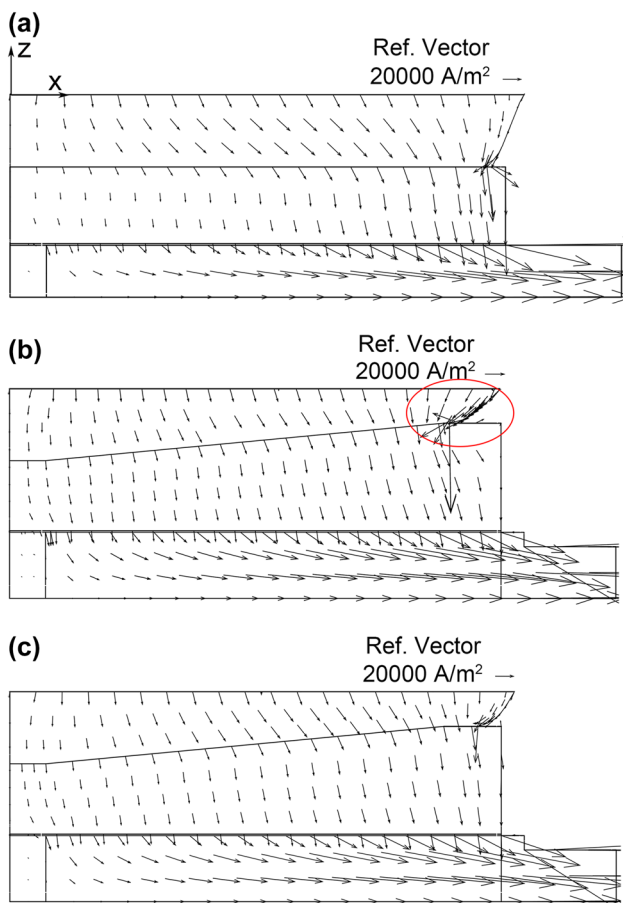


Fig. 4. Current density vector in the cathode assembly. (a) Flat cathode (ACD = 5 cm). (b) Inclined cathode (ACD = 4.5 cm). (c) Inclined cathode (ACD = 4.5 cm, enhanced thermal insulation of sidewall).

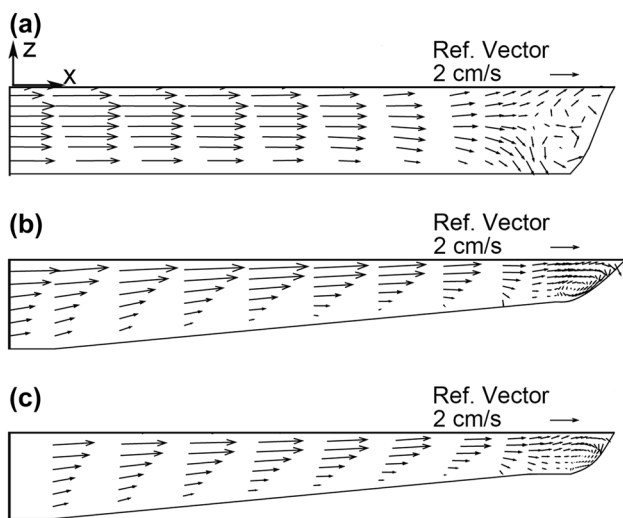


Fig. 5. Cross-section velocity in the metal. (a) Flat cathode (ACD = 5 cm). (b) Inclined cathode (ACD = 4.5 cm). (c) Inclined cathode (ACD = 4.5 cm, enhanced thermal insulation of sidewall).

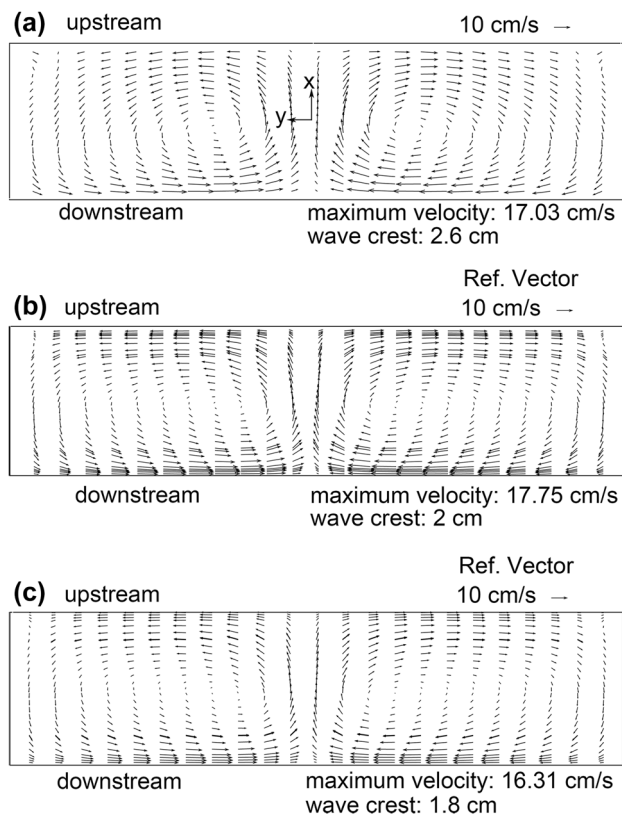


Fig. 6. Metal velocity in the whole cell (4 cm below the bath-metal interface). (a) Flat cathode (ACD = 5 cm). (b) Inclined cathode (ACD = 4.5 cm). (c) Inclined cathode (ACD = 4.5 cm, enhanced thermal insulation of sidewall).

proximity to the ledge, the metal velocity was tiny (Fig. 5c), which was compounded by small eddies that were caused by the ledge blocking to the flow.

The global metal velocity within the cell is shown in Fig. 6. In the absence of enhanced thermal insulation, the maximum velocity of the cell using the inclined cathode (Fig. 6b) was greater than that of the conventional cell (Fig. 6a). It is plausible that the large inverted horizontal current originated from the ledge toe extension. Nevertheless, this large current was not detrimental to the cell as the central metal wave crest was reduced from 2.6 cm to 2 cm. Yet the metal velocity should be kept as small as possible to reduce the metal wave and minimize cathode abrasion. Additionally, larger velocities cause stronger thermal convection within the liquid, which leads to increased heat loss through the sidewall. The ledge profile returned to its desired position with increased thermal insulation, which caused the velocity to decrease and the metal wave crest to reduce to 1.8 cm. The monthly average testing data for the inclined cathode are listed in Table II.

Table II. Testing data of a 300-kA aluminum-reduction cell with modified cathodes

Cell voltage (V)	Metal level (cm)	Current efficiency (%)	Energy consumption (kWh/kg Al)	Cathode voltage drop (mV)	Electrolyte temperature (°C)
3.914	25	89.74	13.00	224	953
3.922	26	90.71	12.88	215	962
3.912	27	91.86	12.69	215	965
3.957	28	92.79	12.71	239	955
3.922	29	92.87	12.58	251	956

For conventional cells in the potline, the average cell voltage and energy consumption were approximately 4.1 V and 13.30 kWh/kg Al, respectively. The modified cathode reduced energy consumption efficiently.

CONCLUSION

A modified cathode with an inclined surface (5° inclination) and increased slot height for the collector bars (230 mm high) was incorporated into two 300-kA industrial aluminum-reduction cells. The cell voltage was reduced by approximately 200 mV compared with a conventional cell with a flat cathode.

The electrothermal distribution was modeled and analyzed using ANSYS, which indicated that the 200-mV cell voltage reduction was caused by a combination of the cathode modification (40 mV) and the reduced electrolyte level (electrolyte depth of 0.5 cm) under the anodes (160 mV).

If the thermal insulation was not changed in the modified cell with a reduced ACD, the ledge toe was extended to the anode shadow by 12 cm, which led to an inverted horizontal current of approximately 7000 A/m² and to an increase in the maximum velocity.

To overcome the lower Joule heating that was caused by the decreased electrolyte levels, the cells were lined with materials with low thermal conductivity. This caused the ledge profile to return to its desired position where the large horizontal current was eliminated. Accordingly, the metal velocity and metal wave in the modified cell were both reduced. Monthly average testing data showed that the modified cathodes saved energy to varying extents, which depended on the metal level.

ACKNOWLEDGEMENTS

The authors are grateful for the financial support from the National Nature Science Foundation of China (Grant No. 51434005), the National Key Technology R&D Program of China (No. 2015BAB04B03), and the Fundamental research funds for the central universities (N15024013 and N162502002).

REFERENCES

- V. Gusberti, D.S. Severo, B.J. Welch, and M. Skyllas-Kazacos, *Light Metals 2102*, ed. C.E. Suarez (Warrendale: TMS, 2012), pp. 929–934.
- D. Whitfield, M. Skyllas-Kazacos, B. Welch, and P. White, *Light Metals 2004*, ed. A.T. Tabbereaux (Warrendale: TMS, 2004), pp. 239–244.
- S. Das, Y. Morsi, and G. Brooks, *JOM* 66, 235 (2013).
- R. von Kaenel and J. Antille, *Light Metals 2011*, ed. S.J. Lindsay (Warrendale: TMS, 2011), pp. 569–574.
- M. Blais, M. Désilets, and M. Lacroix, *Appl. Therm. Eng.* 58, 439 (2013).
- J.M. Dreyfus, L. Rivoaland, and S. Lacroix, *Light Metals 2004*, ed. A.T. Tabbereaux (Warrendale: TMS, 2004), pp. 603–608.
- D. Billinghamurst, B. Paul, G.P. Bearne, and I.A. Coad, *Light Metals 2006*, ed. T.J. Galloway (Warrendale: TMS, 2006), pp. 255–257.
- F. Naixiang, T. Yingfu, P. Jianping, W. Yaowu, Q. Xiquan, and T. Ganfeng, *Light Metals 2010*, ed. J.A. Johnson (Warrendale: TMS, 2010), pp. 405–408.
- Y. Song, J. Peng, Y. Di, Y. Wang, B. Li, and N. Feng, *JOM* 68, 593 (2016).
- L. Xiangpeng, L. Jie, X. Tiepeng, L. Yanqing, and L. Yexiang, *Metall. Ind. Auto.* 4, 30 (2003).
- S. Wilkening and J. Côté, *Light Metals 2007*, ed. M. Sørli (Warrendale: TMS, 2007), pp. 865–873.
- M. Sørli and H.A. Øye, *Cathodes in Aluminium Electrolysis*, 3rd ed. (Düsseldorf: Aluminium-Verlag Marketing & Kommunikation GmbH, 2010), pp. 297–298.
- F. Naixiang, *Aluminum Electrolysis*, 1st ed. (Beijing: Chemical Industry Press, 2006), pp. 297–298.
- A. Khatun and M. Désilets, *Light Metals*, ed. S.J. Lindsay (Warrendale: TMS, 2011), pp. 1035–1040.